Human Molecular Genetics, 2015, Vol. 24, No. 13 3623–3637

doi: 10.1093/hmg/ddv107
Advance Access Publication Date: 20 March 2015
Original Article

ORIGINAL ARTICLE

Impaired retrograde transport by the Dynein/Dynactin complex contributes to Tau-induced toxicity

Malte Butzlaff[1,2,†], Shabab B. Hannan[3,†], Peter Karsten[1], Sarah Lenz[1], Josephine Ng[3], Hannes Voßfeldt[1], Katja Prüßing[1], Ralf Pflanz[4], Jörg B. Schulz[1,5,‡], Tobias Rasse[3,6,‡] and Aaron Voigt[1,‡,*]

[1]Department of Neurology, University Hospital, RWTH Aachen, Germany, [2]Department of Cellular Neurophysiology, Hannover Medical School, Hannover, Germany, [3]Department of Synaptic Plasticity, Hertie-Institute for Clinical Brain Research, University of Tübingen, Germany, [4]Department of Molecular Development Biology, Max-Planck-Institute for Biophysical Chemistry, Göttingen, Germany, [5]JARA – Brain Translational Medicine, Aachen, Germany and [6]Schaller Research Group, University of Heidelberg, Deutsches Krebsforschungszentrum (DKFZ), Proteostasis in Neurodegenerative Disease (B180), Heidelberg, Germany

*To whom correspondence should be addressed at: Department of Neurology, University Hospital, RWTH Aachen, Pauwelsstrasse 30, D-52074 Aachen, Germany. Tel: +49 2418085054; Fax: +49 2418082582; Email: avoigt@ukaachen.de

Abstract

The gene *mapt* codes for the microtubule-associated protein Tau. The R406W amino acid substitution in Tau is associated with frontotemporal dementia with parkinsonism linked to chromosome 17 (FTDP-17) characterized by Tau-positive filamentous inclusions. These filamentous Tau inclusions are present in a group of neurodegenerative diseases known as tauopathies, including Alzheimer's disease (AD). To gain more insights into the pathomechanism of tauopathies, we performed an RNAi-based large-scale screen in *Drosophila melanogaster* to identify genetic modifiers of Tau[R406W]-induced toxicity. A collection of RNAi lines, putatively silencing more than 7000 genes, was screened for the ability to modify Tau[R406W]-induced toxicity *in vivo*. This collection covered more than 50% of all protein coding fly genes and more than 90% of all fly genes known to have a human ortholog. Hereby, we identified 62 genes that, when silenced by RNAi, modified Tau-induced toxicity specifically. Among these 62 modifiers were three subunits of the Dynein/Dynactin complex. Analysis on segmental nerves of fly larvae showed that pan neural Tau[R406W] expression and concomitant silencing of Dynein/Dynactin complex members synergistically caused strong pathological changes within the axonal compartment, but only minor changes at synapses. At the larval stage, these alterations did not cause locomotion deficits, but became evident in adult flies. Our data suggest that Tau-induced detrimental effects most likely originate from axonal rather than synaptic dysfunction and that impaired retrograde transport intensifies detrimental effects of Tau in axons. In conclusion, our findings contribute to the elucidation of disease mechanisms in tauopathies like FTDP-17 or AD.

Introduction

Mutations in the gene *mapt*, which encodes Tau, are associated with frontotemporal dementia with Parkinsonism linked to chromosome 17 (FTDP-17) (1–3). One of these autosomal-dominant, FTDP-17-causing mutations results in the amino acid substitution alanine to tryptophane at position 406 in the Tau protein (Tau[R406W]) (2). Patients with FTDP-17 suffer from disturbed motor skills, behavior and cognition. In post-mortem brains

† These authors contributed equally to this work.
‡ Equally contributing senior authors.

Received: January 19, 2015. **Revised and Accepted:** March 17, 2015

derived from FTDP-17 patients, frontotemporal atrophy and massive loss of neuronal cells are observed. In most FTDP-17 patients, abnormal accumulations of the Tau protein are detected. In the case of Tau[R406W] carriers, these appear to be similar to Alzheimer's filaments (2). Not surprisingly, Tau[R406W] was shown to display an enhanced tendency to form filaments as when compared with wild-type Tau (4). Filamentous deposits of hyperphosphorylated microtubule (MT)-associated protein Tau, the so-called neurofibrillary tangles (NFTs), are cardinal features for several neurodegenerative disorders including Alzheimer's disease (AD) (5–9). NFTs are the common pathological hallmark in all these diseases, which are summarized as tauopathies.

Physiological Tau is associated with MTs, stabilizing the highly dynamic MT network in mature neurons (10–13). In healthy condition, there is an equilibrium between Tau bound and unbound to MTs. In tauopathies, however, a large portion of Tau is hyperphosphorylated and not attached to MT (14,15). Hyperphosphorylated Tau is believed to have high aggregation propensity and accordingly represents the major constituent of NFTs (16). However, it is still elusive how Tau, either native, hyperphosphorylated or aggregated, contributes to neuronal decline.

Several mechanisms to explain the involvement of Tau in neurodegeneration have been discussed to date. Clinical symptoms and neuropathology in post-mortem AD brains correlate with the presence and distribution of NFTs, thus a link between toxicity and the conformational changes in aggregating Tau was presumed (17–20). However, other data suggest that aggregate formation is rather a protective cellular response (21). This hypothesis is supported by the finding that Tau-induced toxicity in mammalian neuronal cell culture in *Caenorhabditis elegans* and *Drosophila melanogaster* occurs without the presence of NFTs (22–25). In addition, it is known that Tau binds to and stabilizes MTs, the main tracks of axonal transport. Increased detachment of Tau causes a destabilization and breakdown of the MT network. In highly compartmentalized neurons with their axonal projections, this will eventually cause an interruption of axonal transport (26–28). In addition to this loss-of-function impact on the MT-based transport, several studies revealed a direct interaction of Tau and axonal transport mechanisms. It has been shown that hyperphosphorylated but still soluble Tau protein is decreasing efficiency of axonal transport *in vivo* (29). Even direct interactions with key players of the transport machineries have already been reported (30).

To gain more insights into these molecular mechanisms, we performed an unbiased genetic screen in *Drosophila*, set to identify modifiers altering Tau toxicity. In the past, *Drosophila* has proved to be a useful model organism to analyze pathomechanisms of human neurodegenerative diseases (31–34). In particular, the short lifespan and availability of genetic tools in *Drosophila* have made it the model organism of choice for identifying genetic interactions. To achieve this, we utilized a library of RNAi lines comprised of almost all fly genes having a human ortholog (35) that covers roughly 50% of all protein coding genes in *Drosophila*. The RNAi lines allowing Gal4-dependent expression of inverted repeat (IR) sequences. Once the IR is transcribed, the resulting RNA forms short hairpins (shRNA). These in turn will be recognized and processed by the endogenous RISC complex, eventually resulting in silencing of the targeted gene by RNA interference (RNAi) (36,37).

Our results suggest that impaired function of transport by the Dynein/Dynactin complex strongly enhances Tau-induced toxicity.

Results

An RNAi screen to identify modifiers of Tau-induced toxicity

Eye-specific (*GMR-Gal4*) expression of Tau[R406W] (*GMR>Tau [R406W]*) resulted in a rough eye phenotype (REP) in adult flies (Fig. 1A). The severity of the Tau-induced REP correlated with the loss of photoreceptors (22) and has been proved to be sensitive readout for genetic modifications (38,39). Thus, we used changes in REP appearance as an indicator for a genetic interaction. In the context of the screen, we first eliminated all RNAi

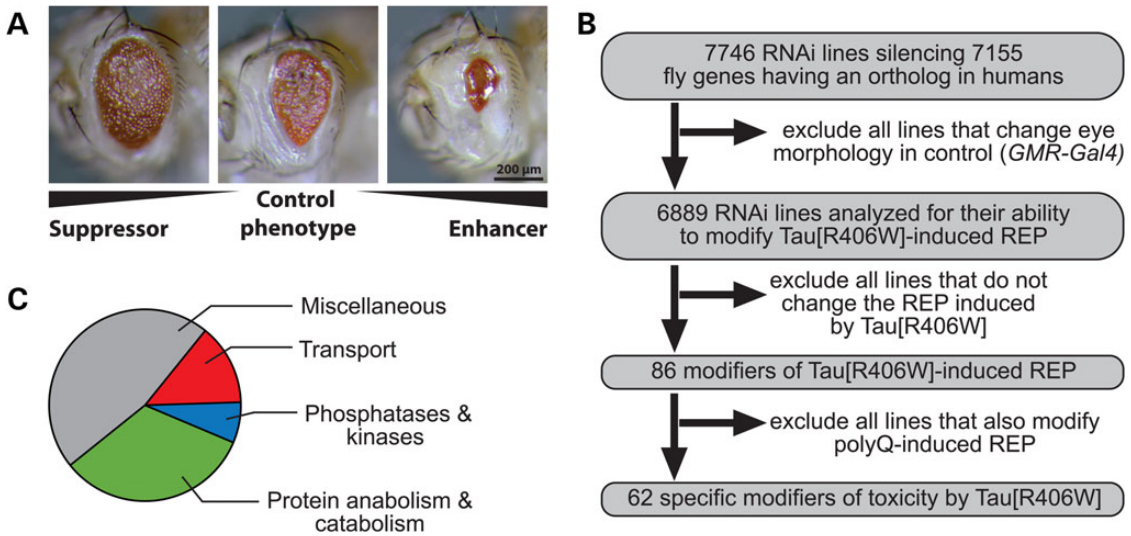

Figure 1. Screening for modifiers of Tau[R406W]-induced toxicity. (**A**) Eye-specific expression of Tau[R406W] induces an REP used as the primary readout for screening (middle). Genetic modifiers were identified based on changes in the Tau[R406W]-induced REP, exemplarily depicted is one suppressor (left) and one enhancer (right). Scale bar indicates 200 µm. (**B**) Flow chart illustrating the accomplished screen including secondary analysis to reduce the number of candidates and to verify identified interactions. (**C**) Gene products encoded by candidate genes were grouped according to assigned gene ontology (GO) terms.

fly lines that after being crossed to *GMR-Gal4* produced offspring with an REP. Using this criterion, 857 lines were excluded as the combined expression with Tau[R406W] would putatively enhance the Tau-induced REP in a non-specific manner. Next, we proceeded with the remaining 6889 lines (Fig. 1B). These lines were crossed with *GMR>Tau[R406W]*, and the F1 generation was screened for robust changes in the Tau-dependent REP. A total of 86 genes were identified to modify Tau[R406W]-induced toxicity when silenced via RNAi. An overview of the primary screen and a brief summary of screen results are depicted in Figure 1B.

Specificity of candidates

Next we wondered whether the identified candidates are specific modifiers of the Tau-induced REP. We were aware of the fact that RNAi-mediated silencing of some genes might render retina cells susceptible to toxic insults. Thus, we assayed our candidates for their ability to modify toxicity induced by proteins/peptides linked to neurodegenerative diseases other than tauopathies. As different disorders usually display different etiologies, we assumed that Tau-specific modifiers should not have an impact on REPs induced by the expression of these proteins/peptides. *GMR-Gal4*-driven expression of a C-terminal fragment of ATXN3 (Ataxin-3) with a stretch of 78 glutamines (polyQ) results in an REP that is sensitive towards genetic modification (35,40–43). Thus, we investigated whether the 86 Tau[R406W] modifiers identified in our screen might have similar effects on the REP, induced by polyQ (Supplementary Material, Fig. S1). We found that the majority of candidates (62 out of 86 modifiers) were uniquely modifying Tau[R406W]-induced toxicity (Fig. 1B). We grouped these specific candidates in functional categories according to assigned Gene Ontology (GO) annotations (Fig. 1C) and identified expected categories (e.g. phosphatases and kinases). An overview of the specific modifiers of Tau[R406W] and assigned GO annotations is provided in Table 1. Twenty-four modifiers similarly effected toxicity caused by Tau[R406W] or polyQ expression. This suggests that silencing these genes might limit overall fitness of cells or impair mechanisms reducing the ability of cells to cope with disease-linked proteins/peptides. To further test this hypothesis, we used the fact that *GMR-Gal4*-driven expression of TAR-DNA binding protein-43 (TDP-43), a protein linked to amyotrophic lateral sclerosis (ALS) and frontotemporal lobal degeneration (FTLD) causes an REP in flies (Supplementary Material, Fig. S1). Indeed, we found that except one, all tested modifiers, which affected Tau- and polyQ-induced phenotypes, similarly enhanced or suppressed TDP-43-induced REPs (Supplementary Material, Table S1).

Toxicity of wild-type and mutant Tau is similarly altered by modifiers

Mutations in *mapt* (e.g. Tau[R406W]) are linked to FTDP-17 with FTLD-tau pathology. To test whether the modifiers identified in our screen specifically alter Tau[R406W]-induced toxicity or represent general modifiers for Tau-induced toxicity, we analyzed the ability of our candidates to also change toxicity induced by overexpression of human wild-type Tau (Tau[WT]). To comparatively analyze the different Tau variants *in vivo*, we first generated new transgenic fly lines by using the ϕ-C31 site-specific recombination (44). By site-specific introduction of transgenic constructs, position effect variegation is minimized resulting in comparable Tau expression levels (Fig. 2A). Driving the expression of either Tau[WT] or Tau[R406W] by *GMR-Gal4*, we observed a moderate REP without any obvious differences in strength (Fig. 2B). Next, all Tau-specific candidates were tested for differences in their ability to modify Tau[WT] and Tau[R406W]-induced REPs. With the exception of *Cwc25* (*CG2843*), all modifiers similarly affected Tau[R406W] and Tau[WT]-induced REPs (not shown). RNAi-mediated silencing of *Cwc25* in combination with Tau[R406W] expression caused lethality in our primary screen and in combination with our site-specific Tau[R406W] transgene. In contrast, silencing of *Cwc25* in Tau[WT] expressing background resulted in viable offspring. Moreover, *Cwc25* silencing did not even enhance the Tau[WT]-induced REP (Fig. 2B).

Silencing members of the Dynein/Dynactin complex enhanced Tau[R406W]-induced REP

Expression of shRNA directed to silence expression of *Dynein heavy chain 93AB* (*dhc93AB*), *Glued* (*p150*) and *Dynamitin* (*p50*) selectively enhanced the Tau-induced REP (Table 1). The corresponding three genes code for key members of the multi-protein Dynein/Dynactin complex, schematically depicted in Figure 3A. In addition, we identified three Dynactin subunits, *p62*, *p25* and *Arp11*, as subtle enhancers of REP. Although the observed subtle modifications did not pass our restrictive thresholds set in the primary screen, an enhancement of the Tau-induced REP by RNAi-mediated silencing of these genes was evident (Fig. 3B). Further, members of the Dynein/Dynactin complex include *Dynein light intermediate chain* (*DLIC*), *Dynein intermediate chain* (*DIC*), *CapZ*, *Arp1* and *p22/24*. Unfortunately, analysis of RNAi lines expressing shRNA specific for *DLIC*, *DIC* and *CapZ* was not possible, because silencing of these genes caused alterations of external eye structures with *GMR-Gal4* alone. There is no RNAi-line available for the *Arp1* ortholog *CG6174* at the Vienna *Drosophila* Resource Center (VDRC) and there is no ortholog of vertebrate *p22/24* in flies. Thus, RNAi lines silencing these genes were not present in our collection. In summary, RNAi-mediated silencing of all tested members of the Dynein/Dynactin complex enhanced the Tau[R406W]-induced REP. Thus, our data strongly suggest that an impairment of the normal function of the Dynein/Dynactin complex aggravates Tau[R406W]-induced REP.

Silencing members of the Dynein/Dynactin complex impairs retrograde axonal transport

The Dynein/Dynactin complex is thought to mediate retrograde transport (46). In order to investigate whether the retrograde transport is impaired in the case of *p50* silencing, we analyzed transport of mitochondria in segmental nerves of *Drosophila* larvae. Mitochondria were chosen to analyze axonal transport impairment. Overexpression of tagged transported cargo proteins might have an effect on overall vesicle abundance, which would falsify our analysis. Monitoring mitochondria movement *in vivo*, we found that upon *p50* silencing, neither the speed nor the rate of transported mitochondria in the anterograde direction was impaired. As expected, the speed of retrograde transported mitochondria was also unaffected. Only the rate of mitochondria transported in the retrograde direction was significantly reduced in the case of *p50* silencing (Fig. 3C). Silencing of $p150^{glued}$, another member of the Dynein/Dynactin complex, had similar effects on transport of mitochondria (not shown). Thus, the reduced rates of retrograde transported mitochondria are most likely due to a reduced abundance of Dynein/Dynactin complexes upon silencing of $p50/p150^{glued}$. Potential off target effects are unlikely, as two independent RNAi lines silencing

Table 1. Specific modifiers of the Tau[R406W]-induced toxicity

No.	Name CG	Effect on Tau	Involved in process	Human ortholog
1	Lerp CG31072	L	Lysosomal transport	IGF2R
2	Dhc93AB CG3723	L	MT-based transport	DNAH17
3	Cwc25 CG2843	L	RNA processing	CWC25
4	– CG3808	L	RNA processing	TRMT2A
5	snRNP-U1-C CG5454	L	Nuclear mRNA splicing	SNRPC
6	– CG5986	L	–	C1orf55
7	fzy CG4274	L	Cell cycle	CDC20
8	Gdi CG4422	L	Signal transduction	GDI1
9	par-6 CG5884	L	Tight junction assembly	PARD6G
10	– CG32442	L	Lipid metabolism	ARV1
11	p150 CG9206	E	MT-based transport	DCTN1
12	p50 CG8269	E	MT-based transport	DCTN2
13	alphaTub84B CG1913	E	MT-based transport	TUBA1A
14	alphaTub67C CG8308	E	MT-based transport	TUBA1C
15	Scamp CG9195	E	Protein transport	SCAMP1
16	g CG10986	E	Vesicle-mediated transport	AP3D1
17	Elongin-B CG4204	E	Gene expression	TCEB2
18	Spp CG11840	E	Membrane protein proteolysis	HM13
19	Prosalpha7 CG1519	E	Protein catabolism	PSMA3
20	Nedd8 CG10679	E	Proteolysis	NEDD8o
21	Fer1 CG10066	E	Regulation of transcription	PTF1A
22	– CG10979	E	Regulation of transcription	ZNF800
23	– CG17327	E	Translation	PTRH2
24	hipk CG17090	E	Protein phosphorylation	HIPK2
25	– CG32666	E	Protein phosphorylation	STK17A
26	– CG6330	E	Uridine metabolism	UPP2
27	Su(z)2 CG3905	E	Brain development	BMI1
28	Flo-2 CG11547	E	Cell adhesion	FLOT2
29	– CG7896	E	Cell adhesion	IGFALS
30	– CG8664	E	Cytoskeleton organization	PCLO
31	Snp CG44248	E	Exonuclease activity	ERI2
32	Apf CG31713	E	Induction of apoptosis	NUDT2

Table continues

Table 1. Continued

No.	Name CG	Effect on Tau	Involved in process	Human ortholog
33	Vha16 CG3161	E	Insulin receptor signaling	ATP6V0C
34	Vha36 CG8186	E	Insulin receptor signaling	ATP6V1D
35	– CG14184	E	Lysosome organization	LAMTOR1
36	krz CG1487	E	MAPK signaling pathway	ARRB1
37	Dab CG9695	E	Nervous system development	DAB1
38	T3dh CG3425	E	Oxidation–reduction process	ADHFE1
39	– CG3500	E	Regulation of apoptosis	TEX261
40	GstS1 CG8938	E	Glutathione metabolization	HPGDS
41	– CG7433	E	Amino acid metabolization	ABAT
42	Cyp301a1 CG8587	E	Tergite morphogenesis	CYP24A1
43	ttv CG10117	E	Heparan sulfate proteoglycan biosynthesis	EXT1
44	– CG8785	E	Amino acid transmembrane transport	SLC36A4
45	– CG32479	E	Ubiquitin-dependent protein turnover	USP10
46	– CG42788	S	Regulation of synapse plasticity	FRMPD4
47	– CG18508	S	Signal transduction	C18orf32
48	nord CG30418	S	Extracellular matrix organization	C4orf31
49	Mad1 CG2072	S	Cell cycle	MAD1L1
50	Shroom CG34379	S	Cell morphogenesis	SHROOM3
51	– CG31259	S	–	TMEM135
52	– CG5500	S	–	C17orf90
53	hep CG4353	S	Protein phosphorylation	MAP2K7
54	– CG6418	S	Protein localization	DDX42
55	– CG31534	S	Protein ubiquitination	LMO7
56	– CG32351	S	Proteolysis	LAP3
57	– CG14621	S	Transport	SLC35E1
58	Nuf2 CG8902	S	Neurogenesis	
59	– CG43444	S	–	TET1
60	– CG32809	S	–	
61	– CG3511	S	Protein folding	PPWD1
62	– CG15629	S	Metabolic	DHRS3

Table lists gene names (if applicable) and gene ID of all identified specific modifiers of the Tau[R406W]-induced REP. A brief summary of the molecular and biological functions assigned to the identified fly gene products (flybase) is given. In addition, the names of the human homolog (as listed in the HomoloGene database) are also indicated. S, suppressor; E, enhancer; L, lethal.

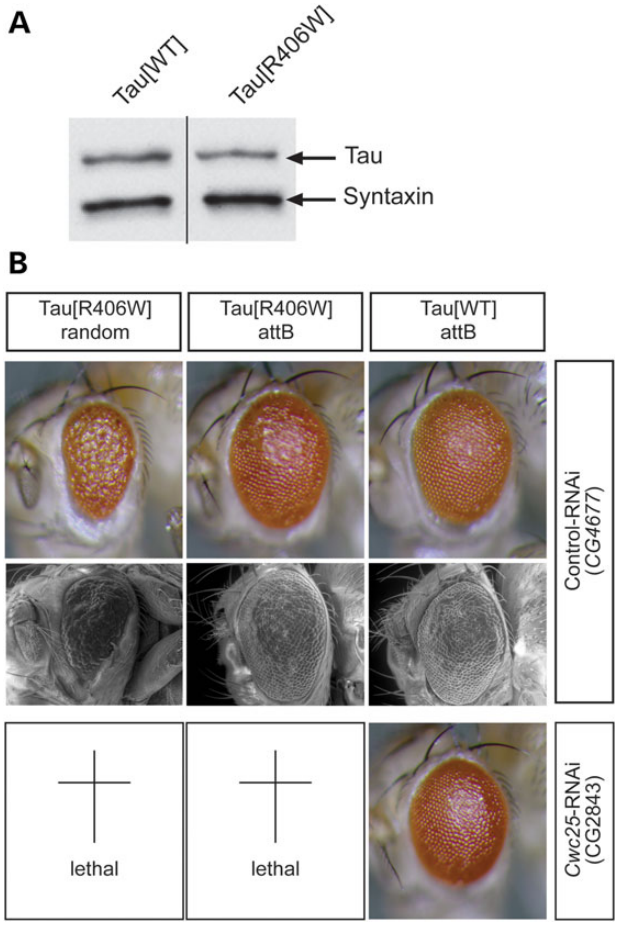

Figure 2. Silencing *Cwc25* has different effects on flies expressing Tau[WT] or Tau [R406W]. (**A**) Western blot demonstrating comparable Tau levels in fly head lysates derived from flies with either Tau[WT] or Tau[R406W] expression. (**B**) Light micrographs (LM) and SEM of flies with eye-specific expression of indicated Tau variants. The Tau[R406W]-expressing fly line used for screening displays high Tau levels and induces an obvious REP (left). In the absence of concomitant shRNA expression, flies with identical Tau[WT] and Tau[R406W] expressions (site-directed insertions) show similar REPs (upper rows). Simultaneous silencing of *Cwc25* by RNAi has no impact on the Tau[WT]-induced REP, whereas *Cwc25* silencing in combination with Tau[R406W] expression results in lethality (lower row). *GMR-Gal4* was used to activate UAS-dependent expression (A and B).

p50 and $p150^{glued}$ caused reduced rates of retrograde transported mitochondria.

Tubulin network in axons is unaffected by silencing members of the Dynein/Dynactin complex and concomitant Tau[R406W] expression

The observed enhancement of Tau[R406W]-induced toxicity could be a consequence of a destabilized MT network by RNAi-mediated impairment of the retrograde transport. However, the anterograde transport was not affected by silencing of *p50* (Fig. 3C). Anterograde transport is mediated by the MT network and would have been impaired in the case of MT breakdown. In addition, staining of segmental nerves in third-instar larvae expressing Tau[R406W] in combination with RNAi-mediated silencing of Dynein/Dynactin complex members did not show any obvious changes of the MT network upon Tau[R406W] expression or RNAi-mediated silencing of Dynein/Dynactin complex subunits (Supplementary Material, Fig. S2).

Axons with Tau[R406W] expression and RNAi-mediated silencing of Dynein/Dynactin complex subunits show early signs of axonopathies

Next, we focused on analyzing segmental nerves of these larvae for morphological changes. Impairment of fast axonal transport is known to be accompanied by the formation of axonal swellings, characterized by the local increase in axon diameter and immune reactivity for the membrane marker horseradish peroxidase (HRP). Moreover, an accumulation of axonal cargo inside axonal swellings is observed (47). Staining for HRP and axonal cargo proteins have been successfully used to assay impaired axonal transport in larvae affected by progressive motor neuron disease (48). Although HRP accumulations are seldom detected upon Tau[R406W] expression alone, *p50* silencing in combination with Tau[R406W] expression resulted in HRP-positive areas. In these larvae, increased HRP staining co-localize with axonal accumulation of cysteine string protein (CSP). CSP is a marker of synaptic vesicles (SVs), commonly not enriched in axons (49). Only axonal swelling in segmental nerves of larvae with concomitant *p50* silencing and Tau[R406W] expression showed CSP accumulation (Fig. 4A–C). The observed CSP accumulations were most likely not cumulative but rather synergistic, as they were not observed in the non-combined situation, *p50* silencing or Tau[R406W] expression alone (Fig. 4C).

RNAi experiments can be confounded by off-target effects. Thus, we intended to independently verify our findings by impairing retrograde transport genetically without employing RNAi silencing components of the Dynein/Dynactin complex. To achieve this, we impaired retrograde transport by expression of a dominant negative variant of $p150^{Glued}$ ($p150^{Glued\text{-}DN}$) (50,51). Expression of $p150^{glued\text{-}DN}$ robustly induced HRP immune reactivity (Fig. 4D–F), which was not further increased by concomitant expression of Tau[R406W] and $p150^{Glued\text{-}DN}$ (Fig. 4D). The strong alterations of axonal membranes upon expression of $p150^{glued\text{-}DN}$ compared with *p50* RNAi expression suggest that detrimental effects in larvae with $p150^{glued\text{-}DN}$ expression are more severe.

To score for axonal swellings, we stained larval segmental nerves for the vesicular glutamate receptor (VGlut), another SV protein (52). Although, $p150^{Glued\text{-}DN}$ alone was sufficient to cause a strong increase in HRP immune reactivity in segmental nerves, only a mild accumulation of VGlut was observed. Importantly, these VGlut accumulations were exacerbated by concomitant expression of Tau[R406W] and $p150^{Glued\text{-}DN}$ (Fig. 4D–F). In summary, we observed axonal swelling with cargo accumulations by monitoring two different vesicular proteins, CSP and VGlut. In the presence of Tau[R406W], impairment of retrograde axonal transport by RNAi against *p50* or expression of $p150^{Glued\text{-}DN}$ did exacerbate axonal defects in segmental nerves of *Drosophila* larvae.

Axonal accumulation of synaptic proteins precedes synapse degeneration

The defects in axonal transport might be either the cause or the consequence of impaired synaptic stability. In order to assess the temporal sequence of pathological events, we wanted to analyze the effects of Tau[R406W] expression and concomitant *p50* knockdown on larval neuromuscular junctions (NMJs). First, we quantified the abundance of SV markers at NMJs. Interestingly, Tau[R406W] expression alone led to a significant decrease in

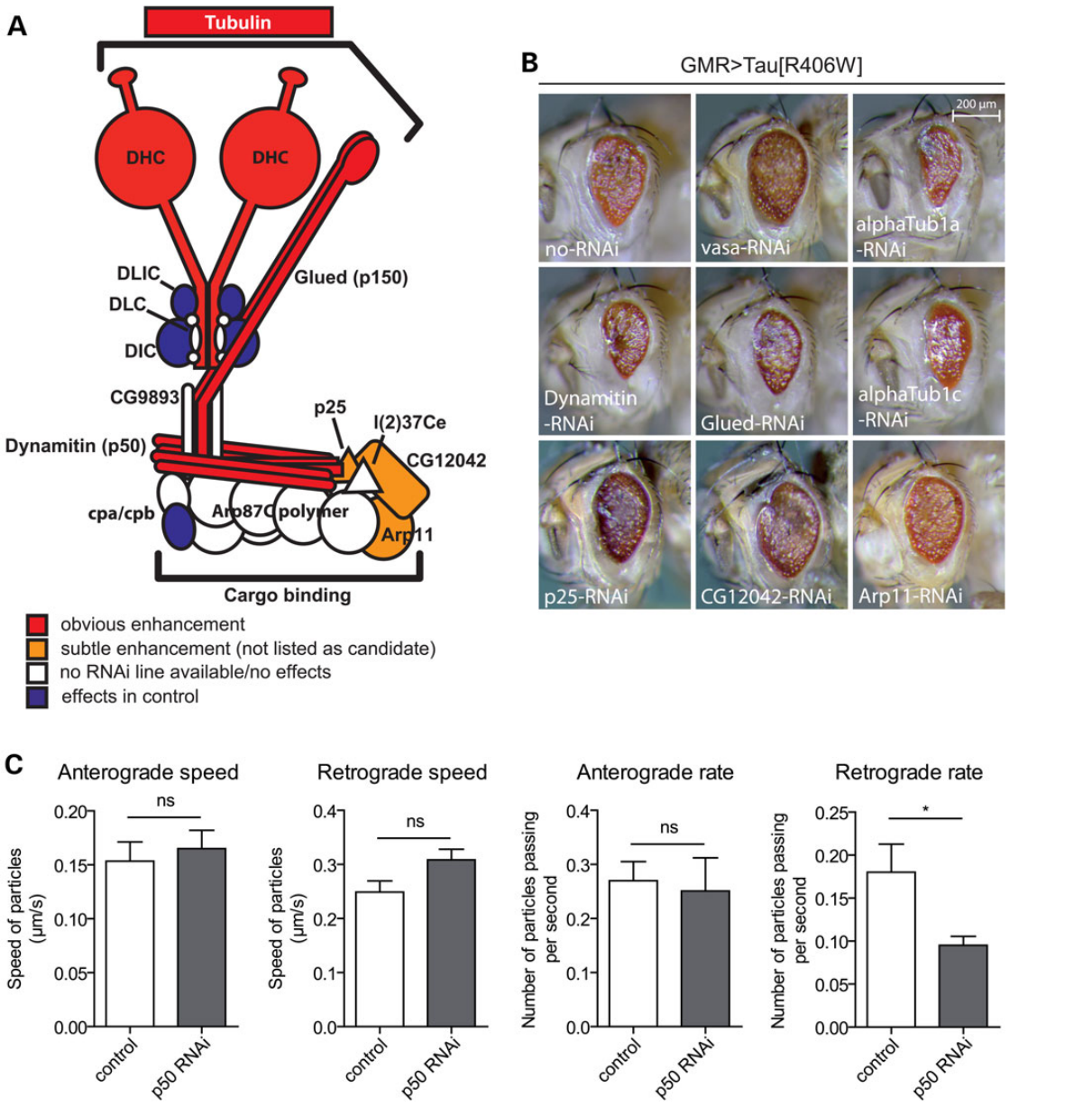

Figure 3. Effects after silencing members of the Dynein/Dynactin complex. (**A**) Schematic representation of the Dynein/Dynactin complex. Dynein subunits and Dynactin subunits are linked by $p150^{Glued}$, an evolutionarily, highly conserved and essential protein in this complex (45). Candidates identified in our screen are marked in red. Gene products that caused only mild changes in the Tau[R406W]-induced REP when silenced by RNAi are marked in orange. Eye-specific (*GMR-Gal4*) silencing of the genes coding for proteins labeled in blue caused alterations of external eye structures or even lethality in the absence of Tau[R406W] confounding an interaction analysis. Gene products labeled in white could not be analyzed for different reasons. (**B**) Exemplified pictures of adult eyes from flies expressing Tau[R406W] and silencing of indicated genes by RNAi under control of the *GMR-Gal4* driver. (**C**) Silencing of *p50* in segmental nerves of L3 larvae reduces rates of retrograde transport. Transport speed and rates of GFP-labeled mitochondria were measured in motor neurons with and without silencing of *p50*. Transport in the anterograde direction was not impaired with regard to speed and rate of transported mitochondria. As expected, *p50* silencing had no effect on the speed of transported mitochondria in the retrograde direction. However, *p50* silencing significantly reduced the rate of retrogradely transported mitochondria. *D42-Gal4* driver was used to achieve UAS-dependent expression of mito-GFP, Tau[R406W] and *p50* RNAi in motor neurons.

the SV proteins CSP and VGlut at the NMJ. The strong reduction in the abundance of SV markers is in agreement with previous data, showing that high levels of Tau protein impair anterograde transport of synaptic cargoes (53). Expression of Tau[R406W] and additional induction of *p50* RNAi did not enhance this decline (Fig. 5A–C). Although there was a clear reduction in the abundance of CSP and VGlut at the NMJ of Tau[R406W] larvae, there were only minor changes in the overall appearance of NMJ (Supplementary Material, Fig. S4).

Silencing members of the Dynein/Dynactin complex and concomitant Tau[R406W] expression did not impair larval locomotion

Nerve terminals of animals expressing Tau[R406W] with concomitant *p50* silencing display a reduced abundance of synaptic proteins, but otherwise appear rather normal with only small morphological alteration in their NMJs. Thus, we investigated whether the changes especially at the axons translate into

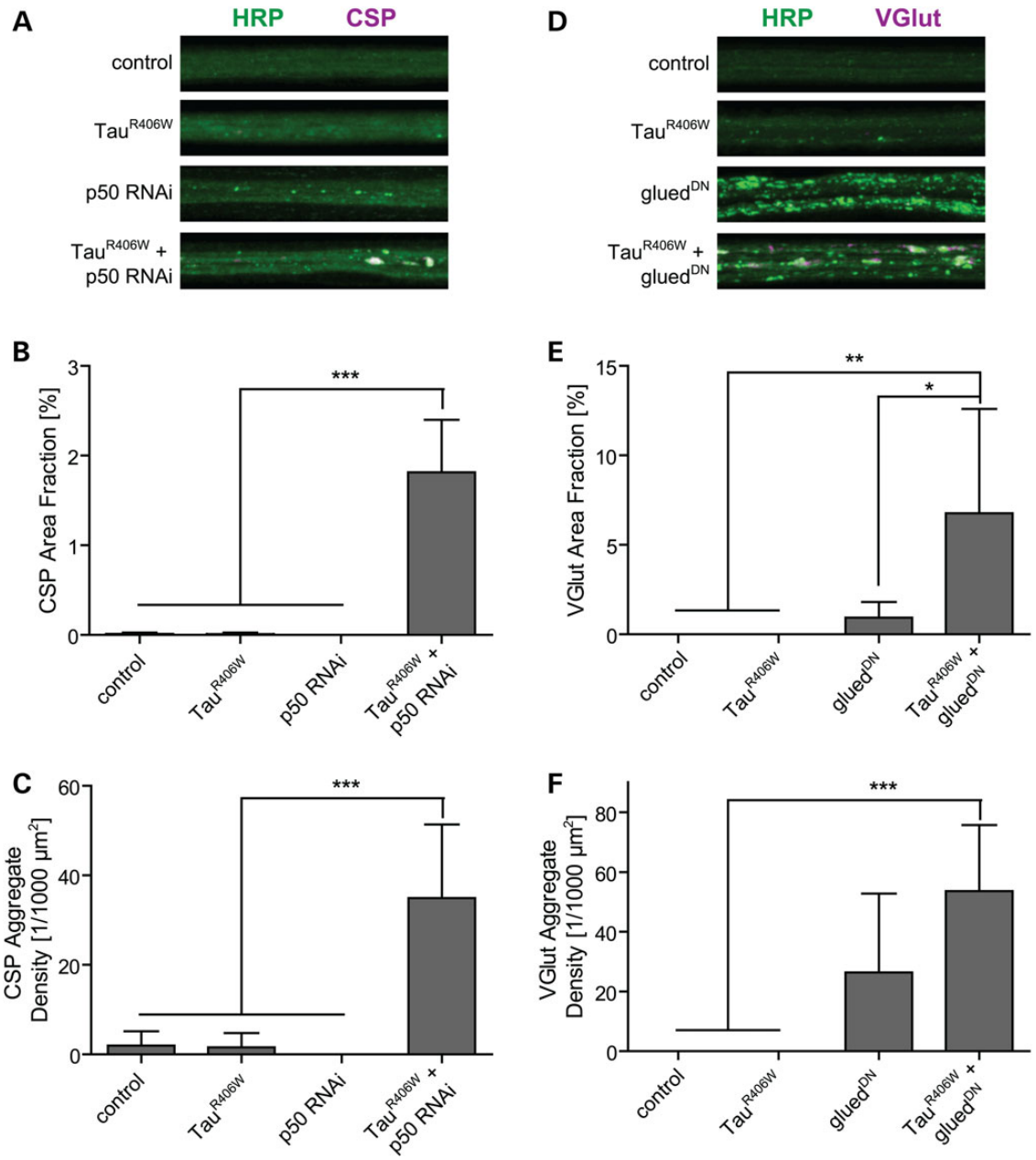

Figure 4. Effect of impaired retrograde transport and Tau[R406W] expression on neuronal integrity and function. (A) Segmental nerves of *Drosophila* larvae expressing indicated transgenes under control of the pan neural driver (*elav-Gal4*, 29°C) were stained with HRP to visualize neuronal membranes (green). Retrograde transport was impaired by either (**A–C**) RNAi-mediated silencing of *p50* or (**D–F**) by expression of a dominant-negative variant of $p150^{Glued}$ (*Glued-DN*). Pathological stages can be estimated by increased HRP fluorescence and the amount of cargo that accumulates in nerves. Although very few HRP punctae were observed in larvae expressing Tau[R406W], or *p50* RNAi alone (A), the expression of *Glued-DN* led to a dramatic increase in HRP punctae (D). Irrespective of the nature of transported cargo proteins (magenta), significant accumulation of (A–C) CSP or (E–G) Vesicular glutamate transporter (VGlut) was only observed upon concomitant Tau[R406W] expression and impairment of retrograde transport. Single-channel pictures of HRP, CSP or VGlut are depicted in Supplementary Material, Figure S3. One-way ANOVA followed by Bonferroni's multiple comparison test. $^{*}P < 0.05$; $^{**}P < 0.01$; $^{***}P < 0.001$.

defects in locomotion. To that end, we performed the righting assay, a sensitive assay to detect minor impairments in motor coordination skills at the larval stage (28,54). Larvae expressing Tau[R406W] or *p50* RNAi alone performed the righting task in the same time as controls. Even the combination of Tau with RNAi silencing *p50* did not cause any changes in righting ability (Fig. 6A). To further probe the fidelity of synaptic function, we investigated larval crawling. We employed a custom-built software (Animaltracer) that allowed us to determine speed and distance travelled by larvae in a unbiased, automated manner (Fig. 6B). We could not detect any significant difference in the locomotion speed between controls and larvae expressing either Tau[R406W] or *p50* RNAi alone or concomitantly. Therefore, we assume that the observed defects in motor neurons in third-instar larvae represent a pre-symptomatic stage of disease without, or only mildly affecting neuronal function. Importantly, at this early stage, mild impairments of the retrograde transport are sufficient to dramatically exacerbate axonal perturbations caused by

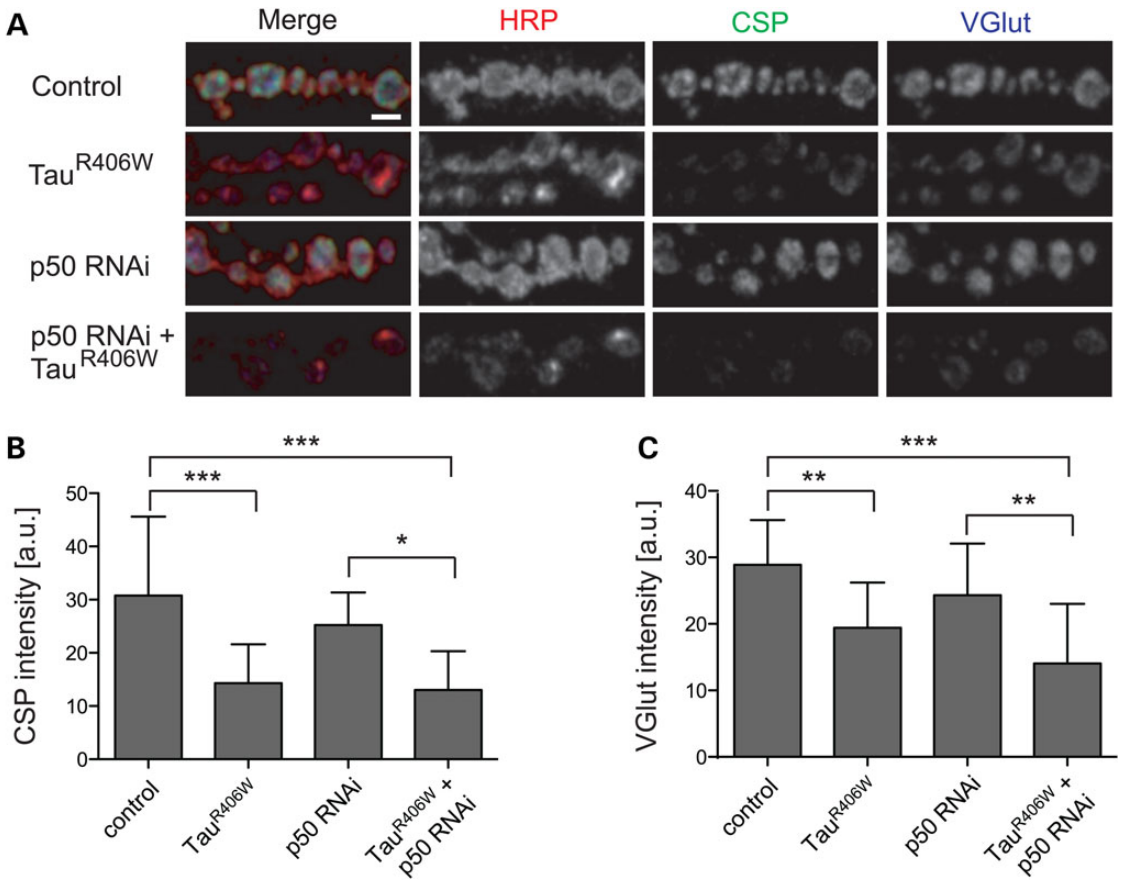

Figure 5. Reduced activity of the Dynein/Dynactin does not affect SV abundance at NMJs. (**A**) NMJs innervating muscle 6/7 in segment A2 and A4 of *Drosophila* larvae expressing indicated transgenes under control of the pan neural driver (*elav-Gal4*, 29°C) were stained to visualize membranes (HRP, red) and two SV markers: CSP (green) and vesicular glutamate transporter (VGlut, blue). Several boutons per NMJ are shown. Scale bar: 5 µm. (**B** and **C**) The abundance of SV proteins (B: CSP, C: VGlut) at the NMJ is decreased in larvae expressing Tau[R406W]. *p50* knockdown alone did not significantly affect SV abundance compared with control. In Tau [R406W]-expressing background, concomitant *p50* silencing did not further decrease SV abundance. One-way ANOVA followed by Bonferroni's multiple comparison test. $^{*}P < 0.05$; $^{**}P < 0.01$; $^{***}P < 0.001$.

ectopic expression of Tau[R406W]. Thus, these changes might be of importance for pathogenesis in tauopathies. Assuming this, the structural alterations on the cellular level observed at a rather early stage of disease should eventually cause dysfunction evident on the organismal level.

Impaired retrograde transport in combination with Tau [R406W] expression causes premature mortality and locomotion defects in adult flies

Pan neural expression of Tau[R406W] and concomitant silencing of *p50* did not cause any locomotion deficits in larvae (Fig. 6). To investigate whether defects arise at later stages, we first analyzed eclosion rates of pupae. Neither pan neural *p50* silencing nor Tau [R406W] expression alone did affect eclosion rates. In contrast, silencing of *p50* in Tau[R406W] expressing larvae strongly reduced eclosion rates (Fig. 7A). This observation confirmed our assumption that the pre-symptomatic signs of neuronal dysfunction become symptomatic over time. However, the pupal lethality prevented us from preforming further analysis using adult flies with pan neural expression.

To address whether there were locomotion defects present in adult flies following expression of Tau[R406W] and concomitant impairment of retrograde transport machinery, we switched to a motor neuron-specific driver (*D42-Gal4*). Using this driver, we found that expression of Tau[R406W] in combination with *p50* silencing had no impact on viability. Thus, we were able to perform climbing assays on aged adult flies. Assaying locomotion of flies with motor neuron-specific expression of Tau[R406W] in combination with *p50* silencing, we observed an age-dependent decline in locomotion skills compared with controls (Fig. 7B). This strongly suggests that cellular changes observed in pre-symptomatic larvae eventually impair neuronal function in adult flies.

Discussion

Drosophila has been successfully used to study tauopathies (22). Utilizing the UAS/Gal4 system (55), several groups have shown that expression of human Tau (wild-type and mutant variants) is detrimental to fly neurons (22,38,39,56). Pan neural expression of Tau reduced the life span of flies accompanied by an age-dependent degeneration of neuronal cell bodies, resulting in vacuolization of the fly brain (22). Thus, Tau expression in flies recapitulates several key features observed in tauopathies (57–59). Moreover, eye-specific expression of Tau caused the so-called REP. The severity of the Tau-induced REP correlates with the loss of photoreceptors and most importantly, Tau-induced REPs are known to be sensitive towards genetic modifiers. Thus, the REPs have been successfully used to identify suppressors and/or enhancers in genetic modifier screens (38,39). In contrast

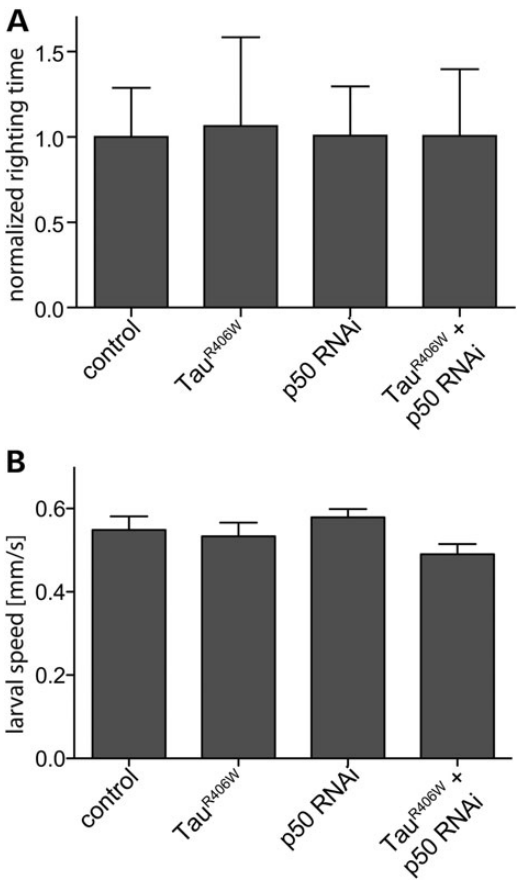

Figure 6. Analysis of fly larvae. Plotted is (**A**) the time interval of an upside down turned larva needs to get back to an upright position (righting time) normalized to control and (**B**) larval speed. Assaying indicated genotypes, including larvae with Tau[R406W] expression in combination with impaired retrograde transport (*p50* RNAi), revealed no significant differences (one-way ANOVA followed by Bonferroni's multiple comparison test) between tested genotypes. Pan neural driver *elav-Gal4* was used to drive expression and *white*-RNAi served as control (A and B). Number of larvae analyzed was $n > 20$ (A) and averages of six movies per genotype monitoring up to 200 larvae per movie (B).

to our work where we used Tau[R406W], previous screens used expression of either wild-type Tau or Tau[V337M] to induce an REP. An additional difference between former screens and ours is the selection of modifier libraries used. So far, rather small collections of transposable elements covering a maximum of 2000 fly genes were used. In contrast, our screen utilized a library of RNAi lines comprised of almost all fly genes having a human ortholog (35). There are well-known drawbacks of using RNAi, mainly possible off-target effects and the ambiguous efficacy of gene silencing. However, the almost genome-wide coverage by the VDRC collection and the availability of sub-libraries like the "human ortholog" selection used here predominate these drawbacks. We screened roughly 50% of all protein coding genes of the fly genome. The specificity of our assays is highlighted by the fact that only a small number of genes (<1% of all genes analyzed) were identified to modify toxicity induced by Tau[R406W]. Cross-validation of identified candidates with previous screens performed in our laboratory revealed specific modifiers of Tau [R406W] toxicity, as they neither affected polyQ-induced REP nor changed RNAi-expression eye morphology *per se*. The mutant Tau[R406W] variant used in our screen is linked to FTDP-17. Evaluation of our candidates showed a common effect towards wild-type and the R406W mutant Tau variant. Except for *Cwc25*, all identified candidates might have a general implication in tauopathies, regardless of any disease-causing Tau mutation. *Cwc25* is conserved among species from yeast to human. However, functional information on CWC25 protein is limited. Yeast-derived data suggest that CWC25 is part of the spliceosome and takes part in the initial steps of exon splicing (60,61). In our analysis, cDNA constructs were used for Tau expression. Thus, effects of splicing on Tau expression and abundance are unlikely. For this reason, we desisted from further analysis of *Cwc25* in the context of Tau-induced toxicity.

In relation to other modifier screens of Tau-induced neurodegeneration, we report a number of novel modifiers not identified in alternative screens (38,39). The differences in modifiers obtained may be attributed to several differences in study design, namely (i) the use of different mutant Tau variants (Tau[WT] or Tau[V337M]), (ii) differences in Tau overexpression by the GAL4/UAS system and (iii) different collections of P-element insertion lines used for screening (i.e. P{EP} and P{Mae-UAS.6.11}). Our modifiers were also largely distinct from those identified in a *C. elegans* model of tauopathy (24,62) (Fig. 8). Despite these differences, also common results were found like proteins of the DDX, SLC and Vha family. Also one kinase, TAOK1 or MARKK, is present in three of the four screens (subtle enhancer in the present screen). These common modifiers demonstrate the significance of the proteins in Tau pathology. In our screen, we identified several lethal interactions: silencing of several candidates caused lethality in combination with Tau expression. This suggests that relatively small changes in the abundance of key protein (function) can strongly modify Tau toxicity. Thus, little alterations in protein function (e.g. by inhibitors) could have enormous effects on Tau-induced toxicity, an encouraging point regarding the development of potential therapeutic treatments. In addition, the results may assist in identifying biomarkers that are predictive of neurodegenerative tauopathies.

Our screen identified several members of the Dynein/Dynactin complex. Especially the key components of the complex, $p150^{glued}$ and p50, were identified as enhancers of Tau-induced toxicity (Fig. 3). Interestingly it was shown that the N-terminal part of Tau directly interacts with $p150^{glued}$ (30). Although the authors found Tau to be responsible for stabilization of Dynein/Dynactin at the MT, our findings suggest a more complex interaction, as the impaired Dynein/Dynactin complex contributes to Tau-induced pathology. Detailed analysis showed that an impaired retrograde transport and concomitant Tau expression caused accumulation of synaptic proteins in axons of segmental nerves (Fig. 4). Interestingly, these accumulations had no major impact on synaptic function, as larval locomotion was not impaired (Fig. 6B). This suggests that we analyzed a presymptomatic stage of tauopathies. Nevertheless, adult flies with Tau[R406W] and concomitant *p50* RNAi displayed a reduction in geotaxis 10 days after eclosion (Fig. 7B).

Alterations in axonal transport are commonly observed in several severe neurodegenerative diseases like ALS (63), spinal muscular atrophy (64), hereditary spastic paraplegia (65), AD (66–68), polyglutamine diseases (69,70), Parkinson's disease (71) and Charcot-Marie-Tooth disease (72–74). Tau, as an MT binding protein, is predominantly present in the axonal compartment, where it binds to and stabilizes MTs, the tracks for transport. Pathological changes in the Tau protein have an impact on the MT-based transport. As MTs serve as the tracks for axonal transport, a decreased efficiency of axonal transport *in vivo* is observed in the presence of hyperphosphorylated Tau (29). On the other hand, an excess of Tau bound to MTs impairs MT-based

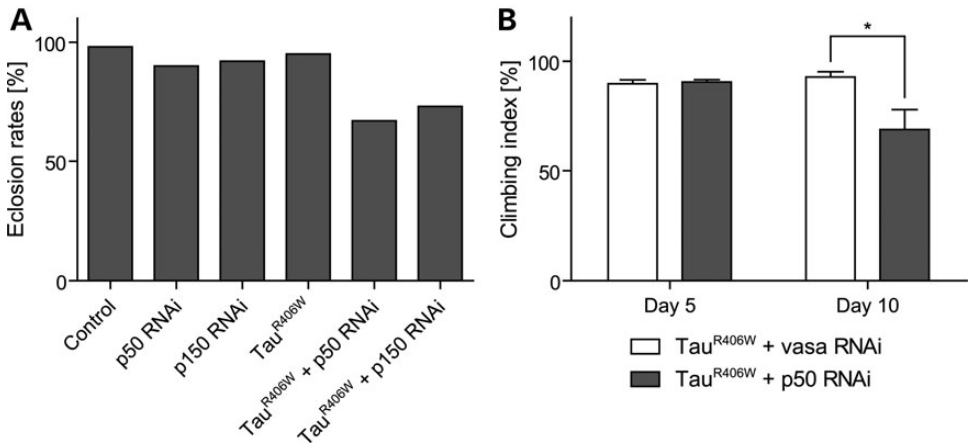

Figure 7. Detrimental effects in adult flies with impaired retrograde transport and Tau[R406W] expression. (**A**) Eclosion rates of flies with pan neural expression of indicated transgenes. Note that only pupae with Tau[R406W] expression and parallel silencing of either *p50* or *p150* displayed a reduced percentage of eclosed adults. (**B**) Climbing index of flies with motor neuron-specific (*D42-Gal4*) expression of Tau[R406W] in combination with RNAi-mediated silencing of either *vasa* (control) or *p50*. No differences was observed 5 days after eclosion, whereas 10 days after eclosion, flies with concomitant expression of Tau[R406W] and *p50* RNAi showed a significant reduction in climbing ability. Two-way ANOVA followed by Bonferroni's multiple comparison test. $^{*}P < 0.05$.

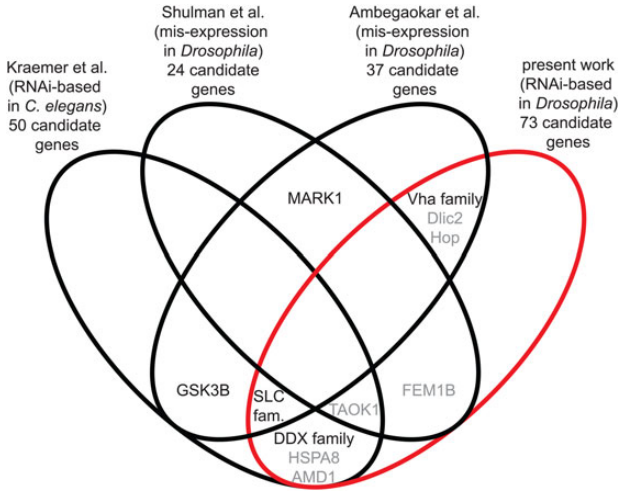

Figure 8. Overlaps between existing and the presented screen for modifiers of Tau-induced pathology. A Venn diagram of the present work (red) and three previous publications of Tau-related modifier-screens: two misexpression-based screens in *Drosophila* (38,39) and an RNAi-based screen in *C. elegans* (62). The mode of modification is not addressed due to differences in model organisms and readout strategies. Modifiers that only show subtle or unspecific effects (in polyQ or TDP43-induced REP) are shown in grey. DDX family, SLC family and Vha family delineate the overlap by two different genes coding for proteins of the same family, respectively.

transport, too. For example, some Kinesin motor proteins (responsible for anterograde transport) are known to pause or even detach from MT due to enhanced interaction with MT-bound Tau. Dynein/Dynactin motor proteins do not detach, but rather show a transient reversal of direction upon interaction with Tau on MTs (75). Hyperphosphorylated Tau decreases transport efficiency *in vivo* (29) and leads to "traffic jams" by disorganized MTs (76). Shifting the ratio of Tau bound or unbound to MT has impact on the MT network of axons and accordingly on axonal transport (59). Phosphorylation of Tau at multiple sites causes its detachment from the MTs. Accumulation of MT detached Tau might also sterically block axonal transport (53). In summary, the detailed mechanisms of how Tau influences motor proteins *in vivo* still remain elusive.

Our findings suggest that an impaired retrograde transport enhances Tau-induced toxicity. Moreover, detailed analysis of segmental nerves and NMJs in *Drosophila* larvae implies that impairment in retrograde axonal transport precedes detrimental changes at the synapse. Although there were only minor defects observed at synapses in larvae with Tau[R406W] expression and concomitant silencing of *p50* (Fig. 5), these larvae showed significantly more axonal abnormalities when compared with controls (Fig. 4). Although axonal and/or synaptic defects will eventually cause neuronal dysfunction, our *in vivo* analysis suggests that—at least in the model used by us—it starts with axonal defects.

In summary, we performed a large-scale, unbiased screen for modifiers of Tau[R406W]-induced toxicity. As a result, we identified a number of known and unknown modifiers. The first proving the robustness of our screening approach, the latter providing insights into new mechanisms contributing to toxicity in tauopathies. Moreover, we show that an impaired retrograde transport strongly enhances Tau-induced toxicity and that detrimental effects first appear in the axonal compartment rather than the synapse.

Materials and Methods

Flies

Flies were raised and maintained on standard cornmeal-agar-yeast food at 25°C. Unless otherwise specified, experiments with *D. melanogaster* larvae and adults were conducted at 25°C. UAS-shRNA fly lines were obtained from the Vienna *Drosophila* Resource Centre (VDRC). A list of VDRC transformant IDs is available on request.

Driver lines:

w[*];P{w[+mC] = Gal4-ninaE.GMR} (BL 1104; *GMR-Gal4* in text); *w[*];;P{w[+mW.hs] = GawB}D42* (BL 8816; *D42-Gal4* in text) and *P{w[+mW.hs] = GawB}elav[C155]* (BL 458, *elav-Gal4* in text) were obtained from Bloomington Stock Centre.

Non-shRNA lines:

w[*];;P{w[+mC] = UAS-hTau[R406W]} (*Tau[R406W]* in text, gift from Mel Feany (22)). *y[*]w[*];;P(acman){w[+] = UAS-Tau[WT]}* and *y[*]w[*];;P(acman){w[+] = UAS-Tau[R406W]}* used to achieve

comparable Tau expression levels (Fig. 2) were generated by BestGene (http://www.thebestgene.com), insertion site 76A2, strain 9732. *w[*];P{w[+mC] = UAS-Hsap\MJD.tr-Q78}c211.2* (BL 8150; referred to in text as *polyQ*), *w[*];P{w[+mC] = UAS-Gl[Delta]}96B* (BL 51645; referred to in text as $p150^{glued DN}$) and *w[1118];P{w[+mW.hs] = GawB}D42,P{w[+mC] = UAS-mito-HA-GFP.AP}3 e[1]/TM6B,Tb[1]* (BL 42737).

Screening

Screening was performed using a screening stock with eye-specific Tau expression (*w;P{w[+mC] = Gal4-ninaE.GMR}*/CyO;*P{w[+mC] = UAS-hTau[R406W]}/TM3*; short *GMR>Tau[R406W]* in text). Female *GMR>Tau[R406W]* flies were crossbred with male flies from the *UAS-shRNA* library and F1 generation was analyzed with regard to changes in the Tau[R406W]-induced REP. At least 10 flies (preferentially five males and females) were used to determine REP severity. Modifiers of the screening phenotype were categorized as suppressors or enhancers, whereas the latter were subdivided into enhancers and lethal interactions. Modifiers were confirmed by at least three biological replicates.

Documentation of compound eye phenotypes

Documentation of compound-eye phenotypes was achieved using an Olympus SZX10 equipped with a SC30 camera and Cell A acquisition software. Selected REPs were documented using scanning electron microscopy (SEM). Unfixed and uncoated flies were imaged using ESEM XL30 FEG scanning electron microscope by FEI, Eindhoven, in "low-vacuum mode" (0.8–1.5 Torr) and an accelerating voltage of 10 kV. Adobe Photoshop was used to rotate and crop images.

Negative geotaxis analysis

Negative geotaxis analysis was performed using male flies raised at 18°C and transferred to 29°C after eclosure. Five and 10 days after eclosion, groups of 10 flies were gently tapped down and the number of flies passing 8 cm height in 10 s was counted (10 repetitions). The minimal number of flies tested per genotype and time point was 44.

Eclosion rates

Eclosion rates indicate the proportion of adult flies hatched from pupae. Flies were allowed to deposit eggs for 24 h in standard food vials. Afterwards, vials were cleared and eggs were placed at 29°C. Upon hatching, adult flies were removed constantly, until flies no longer emerged. Subsequently, eclosed and un-eclosed pupae were counted. Eclosion rates (percent) were calculated by determining the ratio of empty pupae to the total number of pupae in each vial.

Righting assay

Righting assay was performed essentially as previously described (54). In brief, size-matched female L3 larvae were collected and placed for 10 min on an agar plate to acclimatize to the experimental conditions before performing the assay. Larvae were placed upside down on the agar plate, and the total time required to regain normal orientation and to initiate the first contraction wave was recorded. Twenty larvae were analyzed per genotype. Each larva was assayed three times. The average righting time per trial was used for analysis. Data were normalized to control.

Larval locomotion

Larval locomotion defects are tested by larvae locomotion speed and using the righting assay. The larvae locomotion speed was quantified as previously described (48). To measure locomotion speed, we placed up to 200 larvae on a 15 × 15 cm agar plate and filmed for 10 min. Locomotion of the larvae were analyzed with the custom-built software *Animaltracer*. This software was on the basis of the MATLAB software package Worm Tracker & Track Analyzer (Department of Molecular and Cellular Physiology at Stanford University). This algorithm can be divided into two parts: the larval tracker and the track analyzer. The larval tracker identifies and tracks individual larvae within a movie. The track analyzer analyzes the movies and returns the size and the velocity of single larvae. Average locomotion speed is calculated for every movie. Larvae that touched each other were automatically excluded from analysis, and larvae with velocities less than 10% of average velocity of the respective genotype were likewise excluded from analysis. A minimum of six movies per genotype were analyzed. For all further statistical analysis, *n* was defined as the number of movies analyzed.

Western blot

Western blot was performed using fly heads homogenized in radioimmunoprecipitation assay buffer (50 mM Tris, pH 8.0, 150 mM NaCl, 0.1% sodium dodecyl sulfate (SDS), 0.5% sodium deoxycholate, 1× protease inhibitors (Roche), 1% Nonidet P-40). Lysates were separated on 12% gel by SDS–polyacrylamide gel electrophoresis. Proteins were transferred to nitrocellulose membrane. Membrane was blocked with 5% (w/v) skimmed milk Tris-buffered saline containing 0.1% Tween-20. For detection of proteins, the following primary antibodies were used: mouse anti-Tau (1:500) and anti-Syntaxin (1:1000), both obtained from the Developmental Studies Hybridoma Bank (DSHB). Secondary HRP-coupled antibodies (1:10 000, Amersham) were used for chemiluminescence detection (Immun-Star™, WesternC™ Chemiluminescent Kit, BioRad).

Immunohistochemistry

Immunohistochemistry of larval filets was performed as previously described (77). In brief, third-instar larvae were raised at 29°C and cut open along the dorsal midline. After removal of the inner organs, larvae were fixed for 10 min and stained with primary and secondary antibodies. Primary antibodies were applied overnight (4°C) and secondary antibodies were incubated for 2 h at room temperature. The following reagents were used: fixative, 4% paraformaldehyde in phosphate-buffered saline (PBS); washing solution: polybutylene terephthalate (PBT; PBS supplemented with 0.05% Triton X100); and blocking solution: 5% normalized goat serum in PBT. Larval preparations were mounted in Vectashield (Vector Laboratories). Primary antibodies were used in the following dilutions: mouse anti-CSP (DSHB) 1:50, mouse anti-Tubulin (DSHB) 1:100 and rabbit anti-DVGlut (gift from Hermann Aberle) 1:1000. Goat anti-HRP-Cy3 antibody (Dianova) was used at a dilution of 1:500. Secondary antibodies mouse-Alexa-568 and rabbit-Atto 647 (Molecular Probes) were used at a dilution of 1:500.

Illness scores

Illness scores were defined to analyze the integrity of nerve terminals in a double-blinded neurodegenerative scoring paradigm. Here, we took into account occurrence of dystrophic boutons

and inhomogeneity of HRP staining at the NMJs as a measure of the degree of pathological alterations. We assigned an illness score ranging from 0 to 4, with 0 being healthy NMJs with no apparent dystrophic boutons and inhomogeneity of HRP and 4 for most severe degenerative changes as a measure of the degree of neurodegenerative alterations in nerve terminals.

Microscopy and image analysis

Microscopy and image analysis were performed as previously described (48). Samples were imaged on a Zeiss LSM 710 confocal microscope equipped with 405, 445, 488, 514, 561 and 633 Laser Lines and ConfoCor 3 Scanhead. Unless otherwise noted, the following settings were used: objective: 40× plan Apochromat, 1.3 N. A.; Voxel Size: 100 nm × 100 nm × 500 nm; pinhole: 1 AU, average: 2–4. Samples were imaged at the maximum level of brightness, while avoiding saturation. For quantitative comparisons of intensities, common settings were chosen so as to avoid saturation in any of the genotypes. Images were processed as follows: (1) brightness and contrast were adjusted. (2) If appropriate, a Gaussian filter (radius = 2) was applied to the z-stack. (3) Brightness and contrast were adjusted. The relevant slices of the modified stacks were maximum-projected. Projected images were scaled by 2. For better visualization, sometimes a gamma adjustment (gamma = 0.75) was applied as indicated in the figure legend. ImageJ 1.41o, 1.44p or 1.45 s (US National Institutes of Health; http://rsb.info.nih.gov/ij/download.html) was used to process and analyze images.

In vivo imaging

In vivo imaging of transport was essentially performed as previously described (78–80), using a Zeiss LSM 710 confocal microscope equipped with a 40× Plan Apochromat Objective (1.3 N. A.). For better visualization of moving mitochondria, all mitochondria in a 20 µm segment of the nerve were bleached. This allowed for easy visualization of moving particles passing through the bleached region. Imaging was performed in anesthetized larvae using an excitation light of 488 nm wavelength. Range of wavelength absorption: 505–550 nm. The following settings were employed for time series: z-planes: 10; voxel size: 290 nm × 290 nm × 1500 nm, pinhole: 1.6 AU, average: 2, time settings: 150 cycles each being approximately 5 s long.

Statistical analysis

Statistical analysis was calculated using GraphPad Prism software. Plotted is mean and standard deviation (SD). Data were analyzed by either one-way or two-way analysis of variance (ANOVA) followed by Bonferroni's post-hoc test. Only significant differences are marked in figures. $^{*}P < 0.05$; $^{**}P < 0.01$; $^{***}P < 0.001$.

Supplementary Material

Supplementary Material is available at *HMG* online.

Acknowledgements

We thank Christiane Fahlbusch, Kirsten Fladung and Raphael S. Zinser for excellent technical support. In addition, we gratefully appreciate the help of Herbert Jäckle and Mikael Simons at the initial start of this project. We would like to thank Jeannine V. Kern and Jun-yi Zhu for their help in preparing manuscript and Hermann Aberle for providing VGlut antibody.

Conflict of Interest statement. None declared.

Funding

This work was supported by grants of the "Bundesministerium für Bildung und Forschung (BMBF)" within the "Kompetenznetz Degenerative Demenzen (KNDD)" to J.B.S. (grant number 01GI0703) and T.R. (grant number 01GI1005B). A.V. and S.L. were supported by the "Alzheimer Forschungsinitiative (AFI)" (grant number 12812). M.B. was supported by the rebirth cluster of excellence. The funders had no role in study design, data collection and analysis, decision to publish, or preparation of the manuscript.

References

1. Spillantini, M.G., Crowther, R.A., Kamphorst, W., Heutink, P. and van Swieten, J.C. (1998) Tau pathology in two Dutch families with mutations in the microtubule-binding region of tau. *Am. J. Pathol.*, **153**, 1359–1363.
2. Hutton, M., Lendon, C.L., Rizzu, P., Baker, M., Froelich, S., Houlden, H., Pickering-Brown, S., Chakraverty, S., Isaacs, A., Grover, A. *et al.* (1998) Association of missense and 5′-splice-site mutations in tau with the inherited dementia FTDP-17. *Nature*, **393**, 702–705.
3. Poorkaj, P., Bird, T.D., Wijsman, E., Nemens, E., Garruto, R.M., Anderson, L., Andreadis, A., Wiederholt, W.C., Raskind, M. and Schellenberg, G.D. (1998) Tau is a candidate gene for chromosome 17 frontotemporal dementia. *Ann. Neurol.*, **43**, 815–825.
4. Nacharaju, P., Lewis, J., Easson, C., Yen, S., Hackett, J., Hutton, M. and Yen, S.H. (1999) Accelerated filament formation from tau protein with specific FTDP-17 missense mutations. *FEBS Lett.*, **447**, 195–199.
5. Goedert, M., Wischik, C.M., Crowther, R.A., Walker, J.E. and Klug, A. (1988) Cloning and sequencing of the cDNA encoding a core protein of the paired helical filament of Alzheimer disease: identification as the microtubule-associated protein tau. *Proc. Natl Acad. Sci. USA*, **85**, 4051–4055.
6. Kondo, J., Honda, T., Mori, H., Hamada, Y., Miura, R., Ogawara, M. and Ihara, Y. (1988) The carboxyl third of tau is tightly bound to paired helical filaments. *Neuron*, **1**, 827–834.
7. Kosik, K.S., Orecchio, L.D., Binder, L., Trojanowski, J.Q., Lee, V. M. and Lee, G. (1988) Epitopes that span the tau molecule are shared with paired helical filaments. *Neuron*, **1**, 817–825.
8. Wischik, C.M., Novak, M., Thogersen, H.C., Edwards, P.C., Runswick, M.J., Jakes, R., Walker, J.E., Milstein, C., Roth, M. and Klug, A. (1988) Isolation of a fragment of tau derived from the core of the paired helical filament of Alzheimer disease. *Proc. Natl Acad. Sci. USA*, **85**, 4506–4510.
9. Lee, V.M., Balin, B.J., Otvos, L. Jr. and Trojanowski, J.Q. (1991) A68: a major subunit of paired helical filaments and derivatized forms of normal Tau. *Science*, **251**, 675–678.
10. Weingarten, M.D., Lockwood, A.H., Hwo, S.Y. and Kirschner, M.W. (1975) A protein factor essential for microtubule assembly. *Proc. Natl Acad. Sci. USA*, **72**, 1858–1862.
11. Drechsel, D.N., Hyman, A.A., Cobb, M.H. and Kirschner, M.W. (1992) Modulation of the dynamic instability of tubulin assembly by the microtubule-associated protein tau. *Mol. Biol. Cell*, **3**, 1141–1154.
12. Brandt, R. and Lee, G. (1993) Functional organization of microtubule-associated protein tau. Identification of regions which affect microtubule growth, nucleation, and bundle formation in vitro. *J. Biol. Chem.*, **268**, 3414–3419.
13. Trinczek, B., Biernat, J., Baumann, K., Mandelkow, E.M. and Mandelkow, E. (1995) Domains of tau protein, differential

phosphorylation, and dynamic instability of microtubules. *Mol. Biol. Cell*, **6**, 1887–1902.
14. Biernat, J., Gustke, N., Drewes, G., Mandelkow, E.M. and Mandelkow, E. (1993) Phosphorylation of Ser262 strongly reduces binding of tau to microtubules: distinction between PHF-like immunoreactivity and microtubule binding. *Neuron*, **11**, 153–163.
15. Lindwall, G. and Cole, R.D. (1984) Phosphorylation affects the ability of tau protein to promote microtubule assembly. *J. Biol. Chem.*, **259**, 5301–5305.
16. Crowther, R.A. and Goedert, M. (2000) Abnormal tau-containing filaments in neurodegenerative diseases. *J. Struct. Biol.*, **130**, 271–279.
17. Allen, B., Ingram, E., Takao, M., Smith, M.J., Jakes, R., Virdee, K., Yoshida, H., Holzer, M., Craxton, M., Emson, P.C. *et al.* (2002) Abundant tau filaments and nonapoptotic neurodegeneration in transgenic mice expressing human P301S tau protein. *J. Neurosci.*, **22**, 9340–9351.
18. Braak, H. and Braak, E. (1991) Neuropathological staging of Alzheimer-related changes. *Acta Neuropathol.*, **82**, 239–259.
19. Lewis, J., McGowan, E., Rockwood, J., Melrose, H., Nacharaju, P., Van Slegtenhorst, M., Gwinn-Hardy, K., Paul Murphy, M., Baker, M., Yu, X. *et al.* (2000) Neurofibrillary tangles, amyotrophy and progressive motor disturbance in mice expressing mutant (P301L) tau protein. *Nat. Genet.*, **25**, 402–405.
20. Tanemura, K., Murayama, M., Akagi, T., Hashikawa, T., Tominaga, T., Ichikawa, M., Yamaguchi, H. and Takashima, A. (2002) Neurodegeneration with tau accumulation in a transgenic mouse expressing V337M human tau. *J. Neurosci.*, **22**, 133–141.
21. Ross, C.A. and Poirier, M.A. (2005) Opinion: What is the role of protein aggregation in neurodegeneration? *Nat. Rev. Mol. Cell Biol.*, **6**, 891–898.
22. Wittmann, C.W., Wszolek, M.F., Shulman, J.M., Salvaterra, P. M., Lewis, J., Hutton, M. and Feany, M.B. (2001) Tauopathy in *Drosophila*: neurodegeneration without neurofibrillary tangles. *Science*, **293**, 711–714.
23. Fath, T., Eidenmuller, J. and Brandt, R. (2002) Tau-mediated cytotoxicity in a pseudohyperphosphorylation model of Alzheimer's disease. *J. Neurosci.*, **22**, 9733–9741.
24. Kraemer, B.C., Zhang, B., Leverenz, J.B., Thomas, J.H., Trojanowski, J.Q. and Schellenberg, G.D. (2003) Neurodegeneration and defective neurotransmission in a *Caenorhabditis elegans* model of tauopathy. *Proc. Natl Acad. Sci. USA*, **100**, 9980–9985.
25. Shimura, H., Miura-Shimura, Y. and Kosik, K.S. (2004) Binding of tau to heat shock protein 27 leads to decreased concentration of hyperphosphorylated tau and enhanced cell survival. *J. Biol. Chem.*, **279**, 17957–17962.
26. Majid, T., Ali, Y.O., Venkitaramani, D.V., Jang, M.K., Lu, H.C. and Pautler, R.G. (2014) *In vivo* axonal transport deficits in a mouse model of fronto-temporal dementia. *Neuroimage Clin.*, **4**, 711–717.
27. Brunden, K.R., Trojanowski, J.Q., Smith, A.B. III, Lee, V.M. and Ballatore, C. (2014) Microtubule-stabilizing agents as potential therapeutics for neurodegenerative disease. *Bioorg. Med. Chem.*, **22**, 5040–5049.
28. Zhang, B., Carroll, J., Trojanowski, J.Q., Yao, Y., Iba, M., Potuzak, J.S., Hogan, A.M., Xie, S.X., Ballatore, C., Smith, A.B. III *et al.* (2012) The microtubule-stabilizing agent, epothilone D, reduces axonal dysfunction, neurotoxicity, cognitive deficits, and Alzheimer-like pathology in an interventional study with aged tau transgenic mice. *J. Neurosci.*, **32**, 3601–3611.
29. Cowan, C.M., Bossing, T., Page, A., Shepherd, D. and Mudher, A. (2010) Soluble hyper-phosphorylated tau causes microtubule breakdown and functionally compromises normal tau *in vivo*. *Acta Neuropathol.*, **120**, 593–604.
30. Magnani, E., Fan, J., Gasparini, L., Golding, M., Williams, M., Schiavo, G., Goedert, M., Amos, L.A. and Spillantini, M.G. (2007) Interaction of tau protein with the dynactin complex. *EMBO J.*, **26**, 4546–4554.
31. Papanikolopoulou, K. and Skoulakis, E.M. (2011) The power and richness of modelling tauopathies in *Drosophila*. *Mol. Neurobiol.*, **44**, 122–133.
32. Marsh, J.L. and Thompson, L.M. (2006) *Drosophila* in the study of neurodegenerative disease. *Neuron*, **52**, 169–178.
33. Lenz, S., Karsten, P., Schulz, J.B. and Voigt, A. (2013) *Drosophila* as a screening tool to study human neurodegenerative diseases. *J. Neurochem.*, **127**, 453–460.
34. Prüssing, K., Voigt, A. and Schulz, J.B. (2013) *Drosophila melanogaster* as a model organism for Alzheimer's disease. *Mol. Neurodegener.*, **8**, 35.
35. Voßfeldt, S.H., Butzlaff, M., Pru, S.K., Ni Charthaigh, R.A., Karsten, P., Lankes, A., Hamm, S., Simons, M., Adryan, B., Schulz, J.B. *et al.* (2012) Large-scale screen for modifiers of ataxin-3-derived polyglutamine-induced toxicity in *Drosophila*. *PLoS ONE*, **7**, e47452.
36. Buckingham, S.D., Esmaeili, B., Wood, M. and Sattelle, D.B. (2004) RNA interference: from model organisms towards therapy for neural and neuromuscular disorders. *Hum. Mol. Genet.*, **13**(Spec No. 2), R275–R288.
37. Tijsterman, M. and Plasterk, R.H. (2004) Dicers at RISC: the mechanism of RNAi. *Cell*, **117**, 1–3.
38. Shulman, J.M. and Feany, M.B. (2003) Genetic modifiers of tauopathy in *Drosophila*. *Genetics*, **165**, 1233–1242.
39. Ambegaokar, S.S. and Jackson, G.R. (2011) Functional genomic screen and network analysis reveal novel modifiers of tauopathy dissociated from tau phosphorylation. *Hum. Mol. Genet.*, **20**, 4947–4977.
40. Fernandez-Funez, P., Nino-Rosales, M.L., de Gouyon, B., She, W. C., Luchak, J.M., Martinez, P., Turiegano, E., Benito, J., Capovilla, M., Skinner, P.J. *et al.* (2000) Identification of genes that modify ataxin-1-induced neurodegeneration. *Nature*, **408**, 101–106.
41. Kazemi-Esfarjani, P. and Benzer, S. (2000) Genetic suppression of polyglutamine toxicity in *Drosophila*. *Science*, **287**, 1837–1840.
42. Bilen, J. and Bonini, N.M. (2007) Genome-wide screen for modifiers of ataxin-3 neurodegeneration in *Drosophila*. *PLoS Genet.*, **3**, 1950–1964.
43. Lessing, D. and Bonini, N.M. (2008) Polyglutamine genes interact to modulate the severity and progression of neurodegeneration in *Drosophila*. *PLoS Biol.*, **6**, e29.
44. Bischof, J., Maeda, R.K., Hediger, M., Karch, F. and Basler, K. (2007) An optimized transgenesis system for *Drosophila* using germ-line-specific phiC31 integrases. *Proc. Natl Acad. Sci. USA*, **104**, 3312–3317.
45. Karki, S. and Holzbaur, E.L. (1999) Cytoplasmic dynein and dynactin in cell division and intracellular transport. *Curr. Opin. Cell Biol.*, **11**, 45–53.
46. Kardon, J.R. and Vale, R.D. (2009) Regulators of the cytoplasmic dynein motor. *Nat. Rev. Mol. Cell Biol.*, **10**, 854–865.
47. Hurd, D.D. and Saxton, W.M. (1996) Kinesin mutations cause motor neuron disease phenotypes by disrupting fast axonal transport in *Drosophila*. *Genetics*, **144**, 1075–1085.
48. Fuger, P., Sreekumar, V., Schule, R., Kern, J.V., Stanchev, D.T., Schneider, C.D., Karle, K.N., Daub, K.J., Siegert, V.K., Flotenmeyer, M. *et al.* (2012) Spastic paraplegia mutation N256S in the neuronal microtubule motor KIF5A disrupts axonal transport in a *Drosophila* HSP model. *PLoS Genet.*, **8**, e1003066.

49. Zinsmaier, K.E., Hofbauer, A., Heimbeck, G., Pflugfelder, G.O., Buchner, S. and Buchner, E. (1990) A cysteine-string protein is expressed in retina and brain of *Drosophila*. *J. Neurogenet.*, **7**, 15–29.
50. Allen, M.J., Shan, X., Caruccio, P., Froggett, S.J., Moffat, K.G. and Murphey, R.K. (1999) Targeted expression of truncated glued disrupts giant fiber synapse formation in *Drosophila*. *J. Neurosci.*, **19**, 9374–9384.
51. Eaton, B.A., Fetter, R.D. and Davis, G.W. (2002) Dynactin is necessary for synapse stabilization. *Neuron*, **34**, 729–741.
52. Mahr, A. and Aberle, H. (2006) The expression pattern of the *Drosophila* vesicular glutamate transporter: a marker protein for motoneurons and glutamatergic centers in the brain. *Gene Expr. Patterns*, **6**, 299–309.
53. Mandelkow, E.M., Stamer, K., Vogel, R., Thies, E. and Mandelkow, E. (2003) Clogging of axons by tau, inhibition of axonal traffic and starvation of synapses. *Neurobiol. Aging*, **24**, 1079–1085.
54. Zhu, J.Y., Vereshchagina, N., Sreekumar, V., Burbulla, L.F., Costa, A.C., Daub, K.J., Woitalla, D., Martins, L.M., Kruger, R. and Rasse, T.M. (2013) Knockdown of Hsc70–5/mortalin induces loss of synaptic mitochondria in a *Drosophila* Parkinson's disease model. *PLoS ONE*, **8**, e83714.
55. Brand, A.H. and Perrimon, N. (1993) Targeted gene expression as a means of altering cell fates and generating dominant phenotypes. *Development*, **118**, 401–415.
56. Williams, D.W., Tyrer, M. and Shepherd, D. (2000) Tau and tau reporters disrupt central projections of sensory neurons in *Drosophila*. *J. Comp. Neurol.*, **428**, 630–640.
57. Foster, N.L., Wilhelmsen, K., Sima, A.A., Jones, M.Z., D'Amato, C.J. and Gilman, S. (1997) Frontotemporal dementia and parkinsonism linked to chromosome 17: a consensus conference. Conference Participants. *Ann. Neurol.*, **41**, 706–715.
58. Ingram, E.M. and Spillantini, M.G. (2002) Tau gene mutations: dissecting the pathogenesis of FTDP-17. *Trends Mol. Med.*, **8**, 555–562.
59. Brandt, R., Hundelt, M. and Shahani, N. (2005) Tau alteration and neuronal degeneration in tauopathies: mechanisms and models. *Biochim. Biophys. Acta*, **1739**, 331–354.
60. Chiu, Y.F., Liu, Y.C., Chiang, T.W., Yeh, T.C., Tseng, C.K., Wu, N.Y. and Cheng, S.C. (2009) Cwc25 is a novel splicing factor required after Prp2 and Yju2 to facilitate the first catalytic reaction. *Mol. Cell. Biol.*, **29**, 5671–5678.
61. Krishnan, R., Blanco, M.R., Kahlscheuer, M.L., Abelson, J., Guthrie, C. and Walter, N.G. (2013) Biased Brownian ratcheting leads to pre-mRNA remodeling and capture prior to first-step splicing. *Nat. Struct. Mol. Biol.*, **20**, 1450–1457.
62. Kraemer, B.C., Burgess, J.K., Chen, J.H., Thomas, J.H. and Schellenberg, G.D. (2006) Molecular pathways that influence human tau-induced pathology in *Caenorhabditis elegans*. *Hum. Mol. Genet.*, **15**, 1483–1496.
63. Williamson, T.L. and Cleveland, D.W. (1999) Slowing of axonal transport is a very early event in the toxicity of ALS-linked SOD1 mutants to motor neurons. *Nat. Neurosci.*, **2**, 50–56.
64. Rossoll, W., Jablonka, S., Andreassi, C., Kroning, A.K., Karle, K., Monani, U.R. and Sendtner, M. (2003) Smn, the spinal muscular atrophy-determining gene product, modulates axon growth and localization of beta-actin mRNA in growth cones of motoneurons. *J. Cell Biol.*, **163**, 801–812.
65. Reid, E. (2003) Science in motion: common molecular pathological themes emerge in the hereditary spastic paraplegias. *J. Med. Genet.*, **40**, 81–86.
66. Ishihara, T., Hong, M., Zhang, B., Nakagawa, Y., Lee, M.K., Trojanowski, J.Q. and Lee, V.M. (1999) Age-dependent emergence and progression of a tauopathy in transgenic mice overexpressing the shortest human tau isoform. *Neuron*, **24**, 751–762.
67. Zhang, B., Higuchi, M., Yoshiyama, Y., Ishihara, T., Forman, M. S., Martinez, D., Joyce, S., Trojanowski, J.Q. and Lee, V.M. (2004) Retarded axonal transport of R406W mutant tau in transgenic mice with a neurodegenerative tauopathy. *J. Neurosci.*, **24**, 4657–4667.
68. Stokin, G.B., Lillo, C., Falzone, T.L., Brusch, R.G., Rockenstein, E., Mount, S.L., Raman, R., Davies, P., Masliah, E., Williams, D. S. *et al.* (2005) Axonopathy and transport deficits early in the pathogenesis of Alzheimer's disease. *Science*, **307**, 1282–1288.
69. Lee, W.C., Yoshihara, M. and Littleton, J.T. (2004) Cytoplasmic aggregates trap polyglutamine-containing proteins and block axonal transport in a *Drosophila* model of Huntington's disease. *Proc. Natl Acad. Sci. USA*, **101**, 3224–3229.
70. Chang, D.T., Rintoul, G.L., Pandipati, S. and Reynolds, I.J. (2006) Mutant huntingtin aggregates impair mitochondrial movement and trafficking in cortical neurons. *Neurobiol. Dis.*, **22**, 388–400.
71. Saha, A.R., Hill, J., Utton, M.A., Asuni, A.A., Ackerley, S., Grierson, A.J., Miller, C.C., Davies, A.M., Buchman, V.L., Anderton, B.H. *et al.* (2004) Parkinson's disease alpha-synuclein mutations exhibit defective axonal transport in cultured neurons. *J. Cell Sci.*, **117**, 1017–1024.
72. Zhao, C., Takita, J., Tanaka, Y., Setou, M., Nakagawa, T., Takeda, S., Yang, H.W., Terada, S., Nakata, T., Takei, Y. *et al.* (2001) Charcot-Marie-Tooth disease type 2A caused by mutation in a microtubule motor KIF1Bbeta. *Cell*, **105**, 587–597.
73. Baloh, R.H., Schmidt, R.E., Pestronk, A. and Milbrandt, J. (2007) Altered axonal mitochondrial transport in the pathogenesis of Charcot-Marie-Tooth disease from mitofusin 2 mutations. *J. Neurosci.*, **27**, 422–430.
74. de Waegh, S. and Brady, S.T. (1990) Altered slow axonal transport and regeneration in a myelin-deficient mutant mouse: the trembler as an in vivo model for Schwann cell-axon interactions. *J. Neurosci.*, **10**, 1855–1865.
75. Dixit, R., Ross, J.L., Goldman, Y.E. and Holzbaur, E.L. (2008) Differential regulation of dynein and kinesin motor proteins by tau. *Science*, **319**, 1086–1089.
76. Shemesh, O.A., Erez, H., Ginzburg, I. and Spira, M.E. (2008) Tau-induced traffic jams reflect organelles accumulation at points of microtubule polar mismatching. *Traffic*, **9**, 458–471.
77. Qin, G., Schwarz, T., Kittel, R.J., Schmid, A., Rasse, T.M., Kappei, D., Ponimaskin, E., Heckmann, M. and Sigrist, S.J. (2005) Four different subunits are essential for expressing the synaptic glutamate receptor at neuromuscular junctions of *Drosophila*. *J. Neurosci.*, **25**, 3209–3218.
78. Fuger, P., Behrends, L.B., Mertel, S., Sigrist, S.J. and Rasse, T.M. (2007) Live imaging of synapse development and measuring protein dynamics using two-color fluorescence recovery after photo-bleaching at *Drosophila* synapses. *Nat. Protoc.*, **2**, 3285–3298.
79. Zhang, Y., Fuger, P., Hannan, S.B., Kern, J.V., Lasky, B. and Rasse, T.M. (2010) *In vivo* imaging of intact *Drosophila* larvae at sub-cellular resolution. *J. Vis. Exp.*, **43**, 2249.
80. Rasse, T.M., Fouquet, W., Schmid, A., Kittel, R.J., Mertel, S., Sigrist, C.B., Schmidt, M., Guzman, A., Merino, C., Qin, G. *et al.* (2005) Glutamate receptor dynamics organizing synapse formation in vivo. *Nat. Neurosci.*, **8**, 898–905.